Investigation of Coumarin Derivative 3-(1-*o*-toluidinoethylidene)-chromane-2,4-dione: IR Spectroscopic Characterization, NBO, and AIM Analysis and Molecular Docking Studies

Edina Avdović[1](✉), Dušan Dimić[2], and Dejan Milenković[1]

[1] Institute of Information Technologies, Department of Science, University of Kragujevac, 34000 Kragujevac, Serbia
edina.avdovic@pmf.kg.ac.rs

[2] Faculty of Physical Chemistry, University of Belgrade, Studentski trg 12-16, 11000 Belgrade, Serbia

Abstract. Various derivatives of coumarin have previously shown a wide range of biological activities. In this contribution, 3-(1-*o*-toluidinoethylidene)-chromane-2,4-dione (**1**) was analyzed by various theoretical techniques in order to understand the potential binding to anti-tumor target agents. The experimental IR spectrum was assigned and compared to theoretical in order to verify the applicability of applied DFT level of theory (B3LYP-D3BJH/6-311+G(d,p)). The Hirshfeld surface analysis (HSA) performed on the crystal structure of title compound allowed the analysis of inter-atomic interactions that lead to the crystal formation. The Natural Bond Orbital (NBO) and Quantum Theory of Atoms in Molecules (QTAIM) gave in-depth insight of the interactions governing the structure of molecule. Molecular docking towards UQCRB protein was used to investigate the possible interactions with proteins. The stability of molecules and various reactive positions make it a potential anti-tumor agent and further experimental studies are needed.

1 Introduction

Coumarin derivatives are compounds that basically contain a simple 2*H*-1-benzopyran-2-one structure. It was first isolated by Vogel in 1820 from Tonka wood in South America [1]. It should be noted that coumarin-based compound daphnin was isolated in 1812, from the plant *Daphne alpina* (*Thimelaeaceae*). However, the structure of that compound, namely (8-hydroxy-7-O-β-D-glucosylcoumarin), was solved in 1830. So today it can be safely said that daphnin was the first isolated coumarin [2–4]. Coumarin derivatives usually occur as secondary metabolites present in different parts of the plants: root, bark, tree, fruit and leaves [5–7]. More than 300 derivatives of coumarin have been identified from different natural sources such as plant families: *Rutaceae*, *Apiaceae*, *Asteraceae*, *Moraceae*, *Leguminosae*, etc. [8–10]. In addition to the plant world, some of the derivatives are isolated from microorganisms and animals [2–4].

N. Filipovic (Ed.): ICCB 2019, LAIS 11, pp. 127–142, 2020.
https://doi.org/10.1007/978-3-030-43658-2_12

Simple coumarin does not have pronounced biological activity, but its derivatives with numerous substituents at various positions such as hydroxyl, alkyl, benzoyl, furanyl, and pyranosyl groups, have a wide range of the biological and pharmacological activities: antibacterial, antifungal, antioxidant, anticoagulant, and cytotoxic [11–14]. In recent years coumarin derivatives have played a significant role in research in biochemistry, medicinal chemistry and bioorganic chemistry, because of their multi-biological activities. For example, it has been found that dicumarol from sweet clover, is a major cause of hemorrhagic disease, deadly to livestock. This compound in the plants is formed by the condensation of two molecules of 4-hydroxycoumarin via formaldehyde. Thanks to intensive research, it has been found that dicumarol has good anticoagulant properties [15]. In addition, numerous hydroxycoumarin derivatives are potential drugs today, they can be used in medicine as anticoagulants, cytostatics, antibiotics, etc. [13, 16–19].

The molecular docking studies have proved as very important tools for the analysis of interactions between coumarin derivatives and biologically important proteins [20, 21]. Ubiquinol-Cytochrome C Reductase Binding Protein (UQCRB) was chosen in this contribution because of its biological importance. This protein is involved in the transfer of electrons across the mitochondrial inner membrane and plays an important role in complex III stability [22]. In recent research, it was presented that down-regulation of this protein inhibits angiogenesis and suggested that UQCRB could be a novel therapeutic target for angiogenesis regulation [23]. The process of angiogenesis is responsible for embryonic development and tissue or organ regeneration. This process is important for the progression of tumors and hepatic fibrosis in pathological conditions, [24]. Application of small bioactive molecules that bind to the UQCRB suppresses hypoxia-induced tumor angiogenesis. This data demonstrates that UQCRB could be applied as a target agent in new approaches for human cancer and mitochondria-related disease investigation [25].

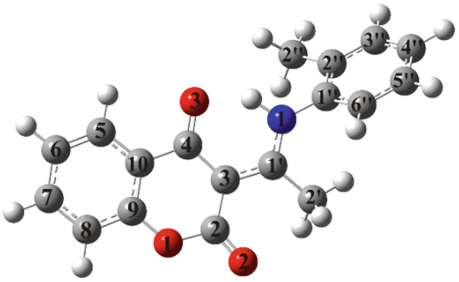

Fig. 1. Structure of 3-(1-*o*-toluidinoethylidene)-chromane-2,4-dione (**1**).

In our previous publications, syntheses of the new derivatives of 4-hydroxycoumarin and their cytotoxic and antimicrobial activity is described [26–31]. Some of these compounds showed excellent cytotoxicity on some cell lines as well as antimicrobial activity on some strains of microorganisms [26–29]. In this paper, due to the significant biological results of similar compounds, the reactivity of 3-(1-(*o*-toluidino)ethylidene)-chroman-2,4-dione (**1**) (Fig. 1) [28] will be tested against the UQCRB protein and analyzed by the Natural Bond Orbital (NBO), Quantum Theory of Atoms in Molecules (QTAIM), and Molecular Docking. Also, a detailed vibration analysis will be described from the

results obtained by comparing the experimental and simulated IR spectra to verify the applicability of the selected level of theory.

2 Materials and Methods

Starting compound 3-(1-o-toluidinoethylidene)-chromane-2,4-dione was obtained as previously explained. The IR spectrum was recorded on the Perkin-Elmer Spectrum One FT-IR spectrometer (KBr pellet technique, 4000–400 cm^{-1}).

Hirshfeld surface analysis was performed using CrystalExplorer17 [32] based on the experimental crystallographic structure of the compound **1** [28]. The geometry units were extracted from crystallographic information files (CIF) obtained from the Cambridge Crystallographic DatabaseCentre (CCDC No. 1817645). The Gaussian 09 program package [33] was used for the optimization of the structure of compound **1** and to create the wavefunction files containing the data needed for the Quantum Theory of Atoms in Molecules (QTAIM) analysis, based on the work of Bader [34, 35]. The Multiwfn program [16] was employed to process the wavefunction files for topology analysis of **1**. In addition, the Natural Bond Orbital analysis (NBO) was done using NBO 5.0 [36]. All density functional theory calculations were performed using the B3LYP-D3BJ functional in combination with a 6-311+G(d,p) basis set.

The AutoDock 4.0 software was used for the molecular docking simulation [37] according to the procedures described elsewhere [38–40]. The three-dimensional crystal structure of UQCRB was obtained from the Protein Data Bank (PDB IDs: 1BCC) [23, 27]. The preparation of protein for docking by removing the co-crystallized ligand, water molecules and co-factors was performed in the Discovery Studio 4.0 [41]. The AutoDockTools (ADT) graphical user interface was used to calculate Kollman charges and to add polar hydrogen. The investigated molecule (**1**) was prepared for docking by minimizing its energy at B3LYP-D3BJ/6-311+G(d,p) level of theory. The molecule was analyzed as a flexible ligand, while the protein remained as a rigid structure in the ADT. All bonds of **1** were set to be rotatable. The Geistenger method for calculation of partial charges was employed. The Lamarckian Genetic Algorithm (LGA) method was employed for protein-ligand flexible docking. For molecular docking simulation, the grid boxes with dimensions 20 Å × 20 Å × 20 Å of UQCRB protein were used in order to cover the protein binding site and accommodate ligand to move freely.

3 Results and Discussion

Vibrational Analysis

The geometry of the examined compound was optimized in the gas phase, using the B3LYP-D3BJ/6–311+G(d,p) theoretical model. It has been previously shown that this level of theory predicts well the vibrational spectra of similar compounds [27, 29]. The IR frequencies were calculated using the same level of theory. The experimental and simulated wavenumbers, together with the assignment, are shown in Table 1. The values of all calculated wavenumbers were higher than the experimental. The reason lies in experimental conditions (KBr pellet) and the fact that theoretical spectra were

simulated for molecules in the gas phase, therefore no intermolecular interactions were considered. The correlation between experimental and theoretical wavenumbers was performed to determine the correction factor. The calculated wavenumbers are scaled using factor 0.9670. The quality of this comparison is evaluated by obtained values of correlation coefficient (R = 0.999) mean absolute error (AAE = 4.26) and mean relative error (ARE = 0.60) which confirm that the theoretical model used describes well the vibrational motion and structure of the molecules (Table 1, Fig. 2).

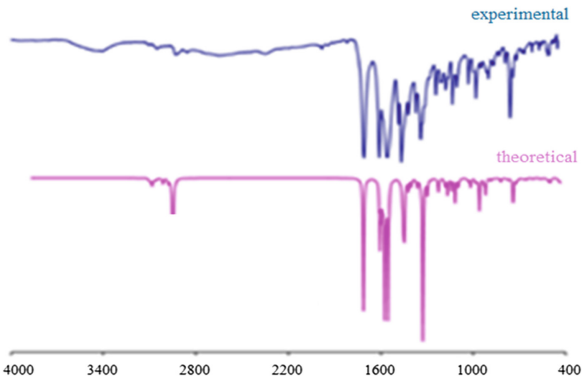

Fig. 2. The experimental and theoretical spectra of the investigated compound (calculated at B3LYP-D3BJ/6-311G+(d,p).

The comparison of theoretical and experimental IR spectra of **1** is shown in Fig. 2. There are three distinct regions in the presented spectra: between 4000 and 2000 cm^{-1}, between 2000 and 1000 cm^{-1}, and below 1000 cm^{-1}. The most pronounced bands in the IR spectrum in the high-frequency region (4000–2000 cm^{-1}) are assigned to different vibrational modes of the C–H and N–H groups. Considering the structure of the examined compound, the band positioned at 3405 cm^{-1} (Table 1) can be assigned to the absorption of hydrogen-bonded N–H group. The moiety O3–C4–C3–C1′–N1–H is observed in structurally similar molecules [26, 27, 29], and it is always described as important for stabilization. This is a so-called hydrogen bond formed by resonance [42]. In the theoretical spectrum the band belonging to N–H vibration is observed at lower wavenumbers due to the fact that molecule was analyzed in the gas phase, therefore no intermolecular interactions were possible. Low-intensity bands that are characteristic of C–H stretching vibrations (aromatic rings I and II, and methyl group) (3107, 3048, 2854, 2350 cm^{-1}) also occur in the high-frequency region (Table 1). The vibration contributions for normal stretching modes (PED values in Table 1), in the range 3405–2350 cm^{-1}, were awarded almost exclusively to N–H and C–H stretching modes (85–99%).

The most intense bands in the IR spectrum can be found in the range 2000–1000 cm^{-1}. These bands are positioned at 1710 cm^{-1} (C=O stretching), 1558 cm^{-1} (C=N stretching), and 1610 cm^{-1} (C–C stretching). Medium and strong bands belong to the bending modes H–C–C (1421 cm^{-1}) and H–C–H (1373 cm^{-1}). Weak bands at

1215, 1179, and 1136 cm^{-1} are assigned to the mixed modes that include C–C stretching, C–N–H and H–C–C bending vibrations. The values of experimental wavenumbers are well-reproduced in the theoretical spectrum with a difference of several cm^{-1}.

Bands that appear below 1000 cm^{-1} can be described as medium and weak. Medium bands are positioned at 904,795, 762, 721 and 669 cm^{-1} and they are due to the mixed vibrational modes including stretching (C–C (acyclic moieties)) and bending (C–C–C, H–C–C, H–C–H, C–N–C, and O–C–O) modes of the first and second benzene ring, aliphatic chain and pyrone ring, as well as combinations of different in-plane and out-of-plane (H–C–C–C, H–C–C–H, O–C–C–C) torsion vibrations. Weak bands are more numerous (Table 1, Fig. 2) and they include some of the previously mentioned vibrational modes.

Table 1. Comparison of the experimental and calculated vibrational wavenumbers and proposed assignments of **1** (scaling factor is 0.9670).

Mode	Experimental wavenumbers	Theoretical wavenumbers (cm^{-1}) B3LYP-D3BJ/6-311+G(d,p)		Vibrational assignments with PED (%)
	IR (cm^{-1})	Unscaled	Scaled	
	3405 w			$\nu_{NH\ (a)}(99)$
105	3107 vw	3207	3101	$\nu_{CH\ (b\text{-}I,\ b\text{-}II)}(99)$
97	3048 w	3158	3054	$\nu_{CH\ (-CH3\ (a))}(90)$
95	2854 w	3115	3013	$\nu_{CH\ (b\text{-}I,\ b\text{-}II)}(90)$
93	2350 w	3064	2963	$\nu_{CH\ (-CH3\ (a))}(85)$
92	1982 w	3050	2949	$\nu_{CH\ (a)}(95)$
90	1710 vs	1771	1713	$\nu_{C=O\ (p)}(90)$
89	1610 vs	1662	1607	$\delta_{CN\ (a)}(50)$
84	1558 vs	1606	1553	$\nu_{CC\ (b\text{-}I)}(50)$
76	1421 m	1470	1421	$\delta_{HCH\ (-CH3\ (a))}(59)$
72	1341 s	1373	1328	$\delta_{HCC\ (b\text{-}I)}(29)$
65	1215 w	1262	1220	$\delta_{CNH\ (a)}(30)$
64	1179 w	1225	1184	$\nu_{CC\ (p)}(48)$
61	1136 w	1181	1142	$\delta_{HCC\ (b\text{-}I)}(32)$
48	951 w	982	949	$\tau_{HCCH\ (b\text{-}I)}(30)$
45	904 m	917	887	$\delta_{CCC\ (p)}(20)$
44	875 w	894	864	$\delta_{CNH\ (a)}(40)$
43	866 w	882	853	$\tau_{HCCC\ (b\text{-}I,\ b\text{-}II)}(25)$
41	832 w	851	823	$\nu_{CC\ (\text{-}CH3\ (a))}(20)$
40	795 m	810	784	$\delta_{HCC\ (b\text{-}II)}(10)$ (b)
39	762 m	801	774	$\tau_{HCCH\ (b\text{-}I)}(40)$
36	721 m	748	723	$\tau_{HCCH\ (b\text{-}II)}(30)$

(*continued*)

Table 1. (*continued*)

Mode	Experimental wavenumbers	Theoretical wavenumbers (cm^{-1}) B3LYP-D3BJ/6-311+G(d,p)		Vibrational assignments with PED (%)
	IR (cm^{-1})	Unscaled	Scaled	
34	689 w	710	687	$\tau_{CCCO\ (p)}(40)$
33	680 w	700	677	$\tau_{HCCH\ (b\text{-}I)}(40)$
32	669 m	694	671	$\delta_{OCO\ (p)}(25)$
30	620 w	637	616	$\delta_{CCC\ (b\text{-}I,\ b\text{-}II)}(20)$
29	574 w	584	565	$\delta_{HCH\ (-CH3\ (a))}(30)$
21	456 w	452	437	$\delta_{HCC\ (b\text{-}II)}(30)$
R				0.999
AAE				4.26
ARE				0.60

a, b-I, b-II, p denote for alkyl side chain, benzene ring (I-first ring attached to pyrone ring and II-second ring attached to N atom) and pyrone moiety, $-CH_3$ stand for methyl moiety, ν – stretching modes; δ – bending modes; τ – torsional modes; vw – very weak; w – weak; m – medium; s – strong; vs – very strong)

Hirshfeld Surface Analysis

Hirshfeld surface analysis (HSA) was first proposed by Spackman and Byrom [43] and comprehensively reviewed in [44]. This method focuses on analyzing the so-called Hirshfeld surface (HS) to reveal weak interactions between monomers in molecular crystal. HSA, in fact, is a kind of inter-fragment (or inter-monomer) surface, which is defined based on the concept of Hirshfeld weight. Probably HS is the most reasonable way to define an inter-fragment surface. Hirshfeld weighting function of an atom can be expressed as:

$$w_A^{\mathrm{Hirsh}}(\mathrm{r}) = \frac{\rho_A^0(\mathrm{r})}{\sum\limits_B \rho_B^0(\mathrm{r})} \tag{1}$$

where ρ_A^0 denotes the density of atom A in free-state. Summing up the weight of all atoms in a fragment yields Hirshfeld weight of this fragment:

$$w_P^{\mathrm{Hirsh}}(\mathrm{r}) = \sum_{A \in P} w_A^{\mathrm{Hirsh}}(\mathrm{r}) \tag{2}$$

HS of fragment P is just the isosurface of $w_P^{\mathrm{Hirsh}} = 0.5$. HSs are built in a crystal structure based on the electron distribution calculated as the sum of spherical electron densities of an atom. Each point on the HSA represents two distances: (1) the distance from the nearest nuclei to the external surface (d_e) and (2) the distance from the nearest nuclei to the internal surface (d_i). The HSA is mapped with the normalized contact distance (d_{norm}) and regions of important intermolecular interactions are presented by

Graphical plots. The value of d_{norm} is represented by red, white, or blue when the intermolecular contacts are shorter, equal, or longer to the vdW separation of nuclei, respectively.

HSA was performed in order to get insight into the role of the intermolecular interaction in the stabilization of **1** via crystal packing. HSA (3D) and fingerprint plots (2D) were drawn by CrystalExplorer17 using an experimental structure input file (CIF) (Fig. 3) [28]. The most significant intermolecular interactions in the crystal lattice of the studied molecule, **1**, are listed in Table 2 and shown in Fig. 3. The intermolecular interactions, such as H···H, O···H and C···H contacts, play a crucial role in the crystal packing of molecule **1.** The H···H intermolecular interactions have the largest contribution in the crystal lattice (50.4%) and they play a major role in crystal lattice stability [45]. The minimum H···H contacts are 2.176 Å for molecule **1** (Table 2 and Fig. 3), respectively. It is important to mention that these contact distances are longer than twice the van der Waals radius of a hydrogen atom. These interactions are represented by a blue color in Fig. 3.

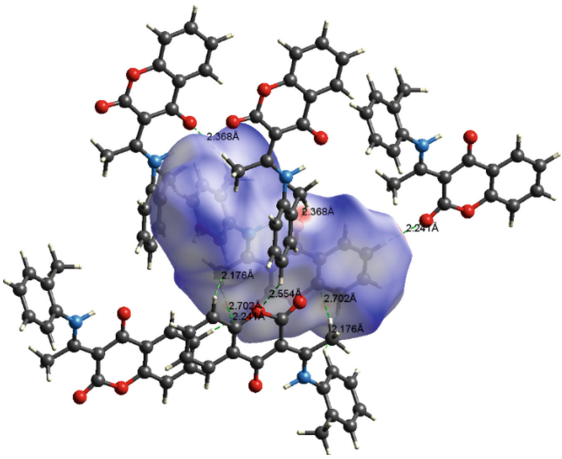

Fig. 3. Graphical plot of the most important intermolecular contacts in **1.**

Table 2. Summary of the most important intermolecular contacts and their percentage contributions in the crystal structure of the studied molecule **1**. The minimum contact distances are in angstroms.

Contacts	%	Contact distances (Å)
C···H/H···C	16.7	2.702
H···H/H···H	50.4	2.176
H···O/O···H	19.4	2.368–2.554

The O···H intermolecular contacts are the second type of close contact that makes a large contribution (19.4%) to the crystal lattice of **1**. The contact distances for these interactions are 2.241, 2.368 and 2.554 Å, respectively. These interactions have shorter contact distances than sums of the van der Waals radius of individual atoms (H and O) and they are represented by red color (Fig. 3).

The H···C intermolecular contacts also showed a high contribution of 16.7% to the overall fingerprint plot. It is found that the minimum contact distance in **1** to be 2.702 Å. This contact is less than the van der Waals radii sum of the C and H atoms with representation by red color (Fig. 3).

Reactivity Parameters, NBO and QTAIM Analysis

In order to evaluate the donor-acceptor interactions in the molecule **1**, the NBO analysis was performed for the investigation of electronic structure [46, 47]. The second-order perturbation theory analysis of the Fock matrix was used. The intramolecular interactions cause the loss of occupancy from the localized NBO of the Lewis structure into an empty non-Lewis orbital. For each donor (i) and acceptor (j), the stabilization energy ($E(2)$) associated with the delocalization between i and j is determined as:

$$E(2) = \Delta E_{ij} = q_i \frac{(F_{ij})^2}{(E_j - E_i)} \tag{1}$$

where q_i is the donor orbital occupancy, E_i, E_j is diagonal elements (orbital energies) and $F_{i,j}$ is the off-diagonal NBO Fock matrix element. It should be pointed out that the higher value of $E(2)$ symbolizes the stronger interaction between electron donors and electron acceptors. The strong intramolecular hyperconjugative interactions obtained by the second-order perturbation theory analysis of the Fock matrix are given in Table 3.

The strongest stabilization interactions are formed within pyrone ring and ethylidene bridge that lead to the stabilization of this part of molecule and cause it planarity. These interactions include π(N–C1″) → π*(C3–C1), π(C3–C1) → π*(O3–C4), π(C3–C1) → π*(O2–C2) and π(C6″–C5″) → π*(N–C1″) with energies between 110.8 and 205 kJ mol^{-1}. The highest value of the interaction energy was calculated for the intramolecular charge transfer from π(C3″–C4″) to C2″ with value of 216 kJ mol^{-1}. The interactions within aromatic rings are also very important for stabilization, as for example π(C7–C8) → π*(C9–C10) with energy 118.2 kJ mol^{-1}.

Additionally, there are strong intermolecular hyperconjugative interactions from (LP2) O1 to π*(C2–O2) and π*(C9–C10), and from (LP2) O2 to σ*(C2–O1) with energies 155.2, 118.3 and 139.3 kJ mol^{-1}, respectively. A strong hydrogen bond (1.63 Å) is formed between N1−H···O3. This result is expected since it is well known that the NH groups are good hydrogen bond donors. On the other hand, the electron pairs on the oxygen of the C=O groups are much better hydrogen bond acceptors than the oxygen of the OH groups. The NBO analysis revealed that the electron density is donated from the p orbitals of the oxygen atom O3 into the proximate σ* antibonding N1–H bond (Table 3). This hydrogen bond additionally stabilizes the structure with 73.8 kJ mol^{-1}. Again, similar was observed for the analogous coumarin derivatives [27, 29] with the interaction energy that is the same, proving that the strength of hydrogen bond is not dependent on substituents. Intermolecular interactions of methyl group also stabilize the

overall structure through LP2(C2″) → π*(N1–C1″) and LP2(C2″) → π*(C3″–C4″) with energies 246.2 and 292.3 kJ mol^{-1}.

Table 3. Some selected second-order interaction energies for **1.**

Donor (i)	Acceptor (j)	E(2)/kJ mol^{-1}	E(j)-E(i)/a.u.	F(i, j)/a.u.
πN1–C1″	π*C3–C1′	205.1	0.32	0.113
πC3–C1′	π*O3–C4	159.2	0.26	0.09
πC3–C1′	π*O2–C2	139.3	0.28	0.087
πC9–C10	π*O3–C4	110.8	0.27	0.076
πC6″–C5″	π*N1–C1″	138.4	0.19	0.085
πC3″–C4″	LP1 C2″	216.0	0.15	0.094
πC7–C8	π*C9–C10	118.2	0.26	0.078
LP2 O3	σ*N1–H	73.8	0.68	0.099
LP2 O1	π*O2–C2	155.2	0.35	0.104
LP2 O1	π*C9–C10	118.3	0.35	0.093
LP2 O2	σ*O1–C2	139.3	0.58	0.126
LP1 C2″	π*N1–C1″	246.2	0.04	0.133
LP1 C2″	π*C3″–C4″	292.3	0.13	0.107

One of the tools for describing various intramolecular interactions is Bader's Quantum Theory of Atoms in Molecules (QTAIM) based on the electron density distribution (ρ) and Laplacian of electron density ($\nabla^2\rho$) at the (3, +1) ring critical points (RCPs) and (3, −1) bond critical points (BCPs) [36]. The important parameters of the stabilization of the investigated molecule are BCPs and RCPs. In this study, the QTAIM analysis was employed for the investigation of the ring and bond critical points between atoms of interest. Two types of interactions exist, the shared interactions (covalent bonds) and closed-shell interactions (ionic bonds, van der Waals bonds and hydrogen bonds). Only the second type of interaction was examined as they additionally stabilize the structure. The value of the electron density of hydrogen bonds is from 0.001 to 0.06 eA with small, but positive Laplacian [21]. On the other hand, the covalent interactions have an electron density of the order of 0.1 eA and negative Laplacian. The RCP is always found within a ring of chemically bonded atoms, and it represents a point within a structure with minimum electron density [22]. BCPs and RCPs can be used as the measure of the strength of the intramolecular hydrogen bond [23, 24] (Table 3).

The rigidity of the coumarin part is proven when properties of RCPs (electron density, Laplacian of electron density, kinetic (G) and potential (V) electron densities) were compared. There are five RCPs, as determined in the Multiwfn program (Fig. 4). Two of RCPs are in aromatic rings, and Table 4 shows that electron density and Laplacian have almost the same values. The parameters of RCP 2 are similar to those for

3-(1-((2-hydroxyphenyl)amino)ethylidene)chroman-2,4-dione also showing that these parameters are not influenced significantly by the substituents on aromatic rings [29]. The third RCP is found in pyrone ring and due to the lack of aromaticity and presence of electronegative atoms, the electron density and Laplacian are lower.

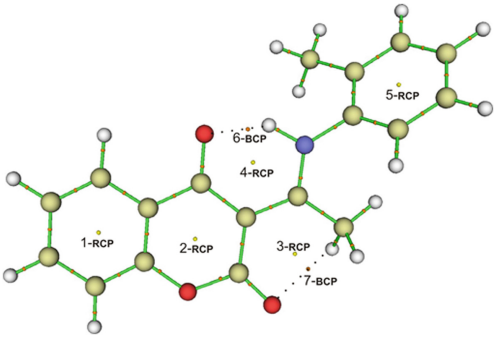

Fig. 4. The BCPs (orange points) and RCPs (yellow points) of the investigated compound.

Two other ring structures are found within the structure of investigated compound. The first one is already mentioned and includes the quasi-six membered ring with hydrogen bond. The value of electron density and Laplacian are 0.0192 eA and 0.128 eA. These values are comparable to those of pyrone ring and again prove the importance of this ring structure for stability of molecule. The values of electron density and Laplacian in BCP between O3 and H are higher than those typically expected for hydrogen bonds, but still lower than those for covalent bonds. The second ring structure is also enclosed by a weak hydrogen bond and it comprises of the following atoms O2–C2–C3–C1′–C2′–H. The value for electron density and Laplacian are 0.0175 eA and 0.070 eA which falls into non-covalent interactions. The methyl group is rotatable therefore it is expected that average values for the parameters are calculated.

Table 4. QTAIM descriptors of molecule **1.**

RCP/BCP No.	ρ	$\nabla^2\rho$	V	G
1	0.0216	0.159	−0.025	0.032
2	0.0192	0.131	−0.021	0.027
3	0.0138	0.075	−0.012	0.015
4	0.0192	0.128	−0.021	0.026
5	0.0215	0.158	−0.024	0.032
6	0.0588	0.165	−0.061	0.051
7	0.0175	0.070	−0.013	0.015

Molecular Docking Analysis

The online server, PASS (Prediction of Activity Spectra for Substances), was designed as a tool for evaluating the general biological potential of an organic drug-like molecule. This server provides simultaneous predictions of many types of biological activity based on the structure of the organic compounds [48, 49]. Some of the possible protein targets of **1** include Membrane integrity agonist, CYP2C12 substrate, Cholestanetriol 26-monooxygenase inhibitor, Ubiquinol-cytochrome-c reductase inhibitor, etc. (Table 5).

The inhibition of **1** towards Ubiquinol-Cytochrome C Reductase Binding Protein (UQCRB) was selected because of the biological importance of this protein and possible role in anti-cancer activity. The value of Pa (probability to be active) for this system is 0.777 (Table 5), as predicted by the PASS analysis. Protein-ligand binding energy and identification of the potential ligand-binding sites were determined from this study as well. These results are given in Table 6 and Fig. 5. The ligand conformation which showed the lowest binding energy (best position) was determined based on the ligand docking results. The position and orientation of ligand inside the protein receptor and the interactions with amino acids that bond to the ligand was analyzed and visualized with Discovery Studio 4.0 and AutoDockTools.

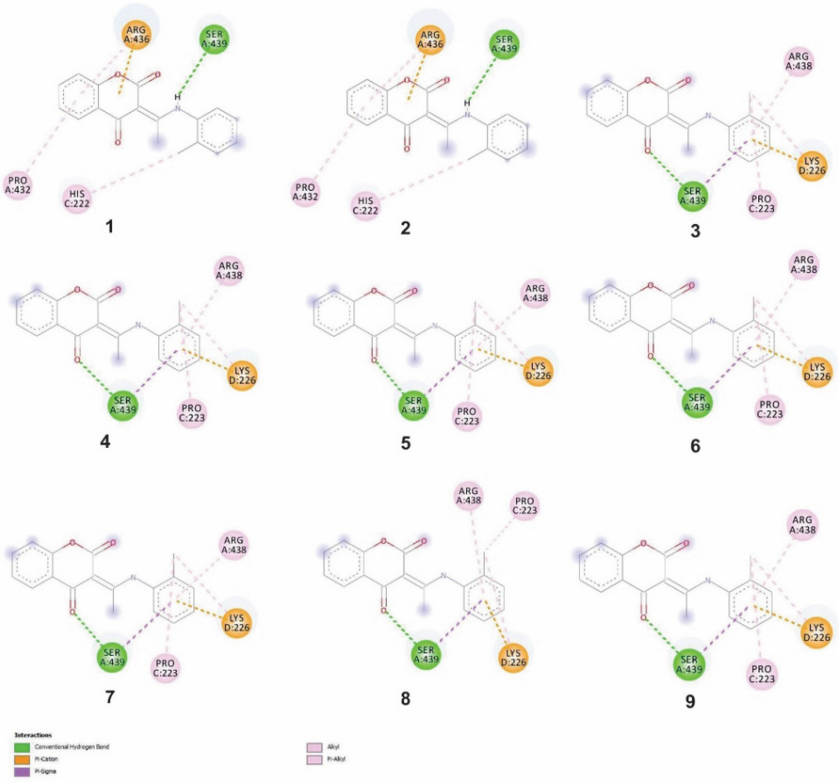

Fig. 5. Docking positions of **1** and UQCRB protein with the lowest energy.

Table 5. PASS prediction for the activity spectrum of **1**.

Pa > 0,7	Pi	Predicted activity
0,827	0,030	Membrane integrity agonist
0,826	0,030	CYP2C12 substrate
0,791	0,004	Cholestanetriol 26-monooxygenase inhibitor
0,799	0,017	CYP2H substrate
0,775	0,004	4-Nitrophenol 2-monooxygenase inhibitor
0,772	0,005	CYP2B5 substrate
0,752	0,010	Oxidoreductase inhibitor
0,777	**0,041**	**Ubiquinol-cytochrome-c reductase inhibitor**
0,710	0,006	General pump inhibitor

Table 6. The estimated values of free energy of binding (ΔG_{bind}, kJ mol^{-1}), binding constants (K_{i}) for various conformations of ligand **1** towards UQCRB protein, distance (Å) and pairwise interaction energies (E_{i}, kJ/mol^{-1}) of H-bonds.

Conformer	ΔG_{bind}, (kJ/mol^{-1})	K_{i} (μM)	H-Bond	Å	E_{i} (kJ/mol)
1	−25.44	35.1	A:SER439:CO---HN:LIG A:SER439:HO---HN:LIG	2.571 2.603	−0.40 −0.36
2	−25.31	37.1	A:SER439:CO---HN:LIG A:SER439:HO---HN:LIG	2.472 2.713	−0.55 −0.25
3	−23.85	66.2	A:SER439:OH---OC:LIG	1.948	−2.45
4	−23.85	66.2	A:SER439:OH---OC:LIG	1.951	−2.44
5	−23.85	66.6	A:SER439:OH---OC:LIG	1.967	−2.39
6	−23.81	66.7	A:SER439:OH---OC:LIG	1.926	−2.50
7	−23.81	68.0	A:SER439:OH---OC:LIG	1.890	−2.52
8	−23.77	68.6	A:SER439:OH---OC:LIG	1.915	−2.52
9	−23.77	68.7	A:SER439:OH---OC:LIG	1.951	−2.44

The results from Table 6 show that very similar values of free energy of binding, between −23.77 and −25.44 kJ mol^{-1}, were obtained for nine conformers. When specific interactions shown in Fig. 5 are observed the relative differences in thermodynamic parameters can be explained. All of the conformers bind to protein with the same interactions, but their energy depends on specific binding site.

The most stable conformer in active position forms two hydrogen bonds with C=O and OH groups of SER439. These bonds have lengths of 2.571 and 2.603 Å and pairwise interaction energies −0.40 and −0.36 kJ mol^{-1}, respectively. ARG436 forms two weak

π-cation and π-alkyl interaction with chroman and benzene rings. On the other hand, HYS222 and PRO432 form weak alkyl-π interaction with the benzene ring of the ligand (Fig. 5).

Other conformers also have hydrogen bonds formed with SER43 which proves the importance of this amino acid for the binding of molecules to the active site of protein. The distance between amino acid and active molecule varies from 1.951 and 2.713 Å. The weaker interactions are formed with ARG436, HIS222, LYS226, and PRO223 through alkyl-π interaction and π-cation interaction. It is assumed that it is actually the number of these weak interactions, not their type that determines the stability of binding. Therefore the most reactive positions, as determined by NBO and QTAIM analyses, are the positions that form interactions with proteins of interest.

4 Conclusions

The experimental and theoretical analysis of coumarin derivative, 3-(1-o-toluidinoethylidene)-chromane-2,4-dione (**1**), was performed. The experimental and theoretical vibrational spectra were compared and it was shown that the correlation between them is 0.999 with the average absolute error of 4.26 cm^{-1}. This was taken as a proof that the selected level of theory, B3LYP-D3BJ/6-311+G(d,p), describes well the experimental structure. The significant intermolecular contacts obtained from Hirshfeld analyses of the solid-state crystal structures of molecule **1** were investigated. The obtained results showed that the H···H intermolecular interactions have the largest contribution in the crystal lattice (50.4%) and they play a major role in crystal lattice stability.

In order to understand the type, nature, and strength of intramolecular interactions in molecule **1,** the AIM and NBO analyses were performed. A particular focus was placed on the characterization of hydrogen-bonding interactions. The NBO analysis exposed that the electron density is donated from the *p* orbitals of the O4 into the σ* antibonding N1–H bond. In this case, the hydrogen bond additionally stabilizes the structure of **1** with 73.8 kJ mol^{-1} and it forms the quasi-six membered ring. The electron density and Laplacian with values of 0.0192 eA and 0.128 eA also show that this bond is stronger than most non-covalent interactions.

The molecular docking study in the active position of UQCRB protein proved that the title molecule forms various interactions with amino acids. All conformers had hydrogen bonds with C=O and OH groups of SER439. What differed various conformers were weak interactions, alkyl-π and π-cation interaction, especially their number with neighboring amino acids. Therefore it was concluded that the stability of molecule and various active positions make it a promising agent for future studies towards anti-tumor agents.

Acknowledgments. This study is supported by the grants from the Ministry of Education, Science and Technological Development of the Republic of Serbia through grants OI172016, OI172015, OI172040, and OI174028.

References

1. Abernethy, J.L.: The historical and current interest in coumarin. J. Chem. Educ. **46**(9), 561 (1969)
2. Murray, R.D.H.: Naturally occurring plant coumarins, pp. 1–119 (1997)
3. Murray, R.D.H.: Naturally occurring plant coumarins, pp. 199–429. Springer, Vienna (1997)
4. Atta-ur-Rahman, Shabbir, M., Ziauddin Sultani, S., Jabbar, A., Iqbal Choudhary, M.: Cinnamates and coumarins from the leaves of *Murraya paniculata*. Phytochemistry **44**(4), 683–685 (1997)
5. Erdelmeier, C., Sticher, O.: Coumarin derivatives from *Eryngium campestre*. Planta Med. **51**(05), 407–409 (1985)
6. Dandriyal, J., Singla, R., Kumar, M., Jaitak, V.: Recent developments of C-4 substituted coumarin derivatives as anticancer agents. Eur. J. Med. Chem. **119**, 141–168 (2016)
7. Magadula, J.J., et al.: Mammea-type coumarins from *Mammea usambarensis* Verdc. Biochem. Syst. Ecol. **56**, 65–67 (2014)
8. Ojala, T., et al.: Antimicrobial activity of some coumarin containing herbal plants growing in Finland. J. Ethnopharmacol. **73**(1–2), 299–305 (2000)
9. Cottigli, F., et al.: Antimicrobial evaluation of coumarins and flavonoids from the stems of *Daphne gnidium* L. Phytomedicine **8**(4), 302–305 (2001)
10. Rosselli, S., et al.: The cytotoxic properties of natural coumarins isolated from roots of *Ferulago campestris* (Apiaceae) and of synthetic ester derivatives of aegelinol. Nat. Prod. Commun. **4**(12), 1701–1706 (2009)
11. Hodák, K., Jakesová, V., Dadák, V.: On the antibiotic effects of natural coumarins. VI. The relation of structure to the antibacterial effects of some natural coumarins and the neutralization of such effects. Cesk. Farm. **16**(2), 86–91 (1967)
12. Cravotto, G., Nano, G.M., Palmisano, G., Tagliapietra, S.: An asymmetric approach to coumarin anticoagulants via hetero-Diels–Alder cycloaddition. Tetrahedron Asymmetry **12**(5), 707–709 (2001)
13. Velasco-Velázquez, M.A., et al.: 4-hydroxycoumarin disorganizes the actin cytoskeleton in B16–F10 melanoma cells but not in B82 fibroblasts, decreasing their adhesion to extracellular matrix proteins and motility. Cancer Lett. **198**(2), 179–186 (2003)
14. Al-Ayed, A., Hamdi, N.: A new and efficient method for the synthesis of novel 3-Acetyl coumarins oxadiazoles derivatives with expected biological activity. Molecules **19**(1), 911–924 (2014)
15. Morrison, S.A., Esnouf, M.P.: The nature of the heterogeneity of prothrombin during dicoumarol therapy. Nat. New Biol. **242**(116), 92–94 (1973)
16. Salinas-Jazmín, N., de la Fuente, M., Jaimez, R., Pérez-Tapia, M., Pérez-Torres, A., Velasco-Velázquez, M.A.: Antimetastatic, antineoplastic, and toxic effects of 4-hydroxycoumarin in a preclinical mouse melanoma model. Cancer Chemother. Pharmacol. **65**(5), 931–940 (2010)
17. Egan, D., James, P., Cooke, D., O'Kennedy, R.: Studies on the cytostatic and cytotoxic effects and mode of action of 8-nitro-7-hydroxycoumarin. Cancer Lett. **118**(2), 201–211 (1997)
18. Finn, G., Creaven, B., Egan, D.: Modulation of mitogen-activated protein kinases by 6-nitro-7-hydroxycoumarin mediates apoptosis in renal carcinoma cells. Eur. J. Pharmacol. **481**(2–3), 159–167 (2003)
19. Joao Matos, M., Vina, D., Vazquez-Rodriguez, S., Uriarte, E., Santana, L.: Focusing on new monoamine oxidase inhibitors: differently substituted coumarins as an interesting scaffold. Curr. Top. Med. Chem. **12**(20), 2210–2239 (2012)
20. Pingaew, R., et al.: Synthesis, biological evaluation and molecular docking of novel chalcone–coumarin hybrids as anticancer and antimalarial agents. Eur. J. Med. Chem. **85**, 65–76 (2014)

21. Liu, X.-H., et al.: Synthesis and molecular docking study of novel coumarin derivatives containing 4,5-dihydropyrazole moiety as potential antitumor agents. Bioorg. Med. Chem. Lett. **20**, 5705–5708 (2010)
22. Cho, Y.S., Jung, H.J., Seok, S.H., Payumo, A.Y., Chen, J.K., Kwon, H.J.: Functional inhibition of UQCRB suppresses angiogenesis in zebrafish. Biochem. Biophys. Res. Commun. **433**(4), 396–400 (2013)
23. Sun, Y., et al.: Identification of UQCRB as an oxymatrine recognizing protein using a T7 phage display screen. J. Ethnopharmacol. **193**, 133–139 (2016)
24. Jung, H.J., Kwon, H.J.: Exploring the role of mitochondrial UQCRB in angiogenesis using small molecules. Mol. BioSyst. **9**(5), 930 (2013)
25. Jung, H.J., Kim, Y., Chang, J., Kang, S.W., Kim, J.H., Kwon, H.J.: Mitochondrial UQCRB regulates VEGFR2 signaling in endothelial cells. J. Mol. Med. **91**(9), 1117–1128 (2013)
26. Dimić, D.S., et al.: Synthesis and characterization of 3-(1-((3,4-dihydroxyphenethyl)amino)ethylidene)-chroman-2,4-dione as potential anti-tumor agent. Oxid. Med. Cell. Longev. **2019** (2019). Article ID 2069250
27. Avdović, E.H., et al.: Synthesis, spectroscopic characterization (FT-IR, FT-Raman, and NMR), quantum chemical studies and molecular docking of 3-(1-(phenylamino)ethylidene)-chroman-2,4-dione. Spectrochim. Acta Part A Mol. Biomol. Spectrosc. **195**, 31–40 (2018)
28. Avdović, E.H., et al.: Preparation and antimicrobial activity of a new palladium(II) complexes with a coumarin-derived ligands. Crystal structures of the 3-(1-(o-toluidino)ethylidene)-chroman-2,4-dione and 3-(1-(m-toluidino) ethylidene)-chroman-2,4-dione. Inorganica Chim. Acta **484**, 52–59 (2019)
29. Avdović, E.H., et al.: Spectroscopic and theoretical investigation of the potential anti-tumor and anti-microbial agent, 3-(1-((2-hydroxyphenyl)amino)ethylidene)chroman-2,4-dione. Spectrochim. Acta Part A Mol. Biomol. Spectrosc. **206**, 421–429 (2019)
30. Avdović, E.H., Milenković, D., Dimitrić-Marković, J.M., Vuković, N., Trifunović, S.R., Marković, Z.: Structural, spectral and NBO analysis of 3-(1-(3-hydroxypropylamino)ethylidene)chroman-2,4-dione. J. Mol. Struct. **1147**, 69–75 (2017)
31. Avdović, E.H., et al.: Synthesis, characterization and cytotoxicity of a new palladium(II) complex with a coumarin-derived ligand 3-(1-(3-hydroxypropylamino)ethylidene)chroman-2,4-dione. Crystal structure of the 3-(1-(3-hydroxypropylamino)ethylidene)-chroman-2,4-dione. Inorganica Chim. Acta **466**, 188–196 (2017)
32. Turner, M.J., McKinnon, J.J., Wolff, S. K., Grimwood, D.J., Spackman, P.R., Jayatilaka, D., Spackman, M.A.: CrystalExplorer17. University of Western Australia (2017)
33. Frisch, M.J., Trucks, G.W., Schlegel, H.B., Scuseria, G.E., Robb, M.A., Cheeseman, J.R., Zakrzewski, V.G., Montgomery, J.J., Stratmann, R.E., Burant, J.C., Dapprich, S., Millam, J.M., Daniels, A.D., Kudin, K.N., Strain, M.C., Farkas, O., Tomasi, J., Barone, V., Cossi, M., Cammi, R., Mennucci, B., Pomelli, C., Adamo, C., Clifford, S., Ochterski, J., Petersson, G.A., Ayala, P.Y., Cui, Q., Morokuma, K., Malick, A.D., Rabuck, K.D., Raghavachari, K., Foresman, J.B., Cioslowski, J., Ortiz, J.V., Baboul, A.G., Stefanov, B.B., Liu, G., Liashenko, A., Piskorz, P., Komaromi, I., Gomperts, R., Martin, R.L., Fox, D.J., Keith, T., AlLaham, M.A., Peng, C.Y., Nanayakkara, A., Challacombe, M., Gill, P.M.W., Johnson, B., Chen, W., Wong, M.W., Andres, J.L., Gonzalez, C., HeadGordon, M., Replogle, E.S., Pople, J.A.: Gaussian 09, Revision B.01. Gaussian Inc., Wallingford (2009)
34. Bader, R.F.W.: A bond path: a universal indicator of bonded interactions. J. Phys. Chem. A **102**, 7314–7323 (1998)
35. Bader, R.F.W.: Atoms in molecules. Acc. Chem. Res. **18**(1), 9–15 (1985)
36. Glendening, E.D., Badenhoop, J.K., Reed, A.E., Carpenter, J.E., Bohmann, J.A., Morales, C.M., Weinhold, F.: NBO 5.0. Theoretical Chemistry Institute, University of Wisconsin, Madison (2001)

37. Morris, G.M., et al.: AutoDock4 and AutoDockTools4: automated docking with selective receptor flexibility. J. Comput. Chem. **30**(16), 2785–2791 (2009)
38. Milenković, D., et al.: Reactivity of the coumarine derivative towards cartilage proteins: combined NBO, QTAIM, and molecular docking study. Monatshefte fur Chemie **149**, 159–166 (2017)
39. Dimić, D., et al.: Experimental and theoretical elucidation of structural and antioxidant properties of vanillylmandelic acid and its carboxylate anion. Spectrochim. Acta Part A Mol. Biomol. Spectrosc. **198**, 61–70 (2018)
40. Dimić, D., Milenković, D., Marković, Z., Marković, J.D.: Structural and spectral analysis of 3-metoxytyramine, an important metabolite of dopamine. J. Mol. Struct. **1134**, 226–236 (2017)
41. BIOVIA Discovery Studio 2016. Accelrys Studio Inc., San Diego (2016)
42. Gilli, G., Bellucci, F., Ferretti, V., Bertolasi, V.: Evidence for resonance-assisted hydrogen bonding from crystal-structure correlations on the enol form of the β-diketone fragment. J. Am. Chem. Soc. **111**, 1023–1028 (1989)
43. Spackman, M.A., Byrom, P.G.: A novel definition of a molecule in a crystal. Chem. Phys. Lett. **267**(3–4), 215–220 (1997)
44. Spackman, M.A., Jayatilaka, D.: Hirshfeld surface analysis. CrystEngComm **11**(1), 19–32 (2009)
45. Grabowsky, S., Dean, P.M., Skelton, B.W., Sobolev, A.N., Spackman, M.A., White, A.H.: Crystal packing in the 2-R,4-oxo-[1,3-a/b]-naphthodioxanes – hirshfeld surface analysis and melting point correlation. CrystEngComm **14**(3), 1083–1093 (2012)
46. Dimić, D., Petković, M.: Control of a photoswitching chelator by metal ions: DFT, NBO, and QTAIM analysis. Int. J. Quantum Chem. **116**, 27–34 (2015)
47. Dimić, D.: The importance of specific solvent–solute interactions for studying UV–vis spectra of light-responsive molecular switches. Comptes Rendus Chim. **21**(11), 1001–1010 (2018)
48. Khurana, N., Ishar, M.P.S., Gajbhiye, A., Goel, R.K.: PASS assisted prediction and pharmacological evaluation of novel nicotinic analogs for nootropic activity in mice. Eur. J. Pharmacol. **662**(1–3), 22–30 (2011)
49. Goel, R.K., Singh, D., Lagunin, A., Poroikov, V.: PASS-assisted exploration of new therapeutic potential of natural products. Med. Chem. Res. **20**(9), 1509–1514 (2011)